

# An analysis of covariant Lyapunov vectors in Hamiltonian dynamical systems

Jason R. Green,<sup>1,2,\*</sup> David J. Wales,<sup>1,†</sup> and R. Stephen Berry<sup>2,‡</sup>

<sup>1</sup> *Department of Chemistry, University of Cambridge,  
Lensfield Road, Cambridge CB21EW, United Kingdom*

<sup>2</sup> *Department of Chemistry, The University of Chicago,  
and The James Franck Institute, Chicago. Illinois 60637, USA*

(Dated: February 22, 2010)

Finite-time Lyapunov exponents of chaotic dynamical systems depend quantitatively and qualitatively on the tangent bundle vector field. Here, two vector sets used in numerical calculations, namely the Gram-Schmidt vectors and the covariant Lyapunov vectors, are compared for a Hamiltonian dynamical system. Trajectories of a model, three-atom Lennard-Jones cluster are simulated and partitioned into uniform time segments of varying length. Distributions of finite-time Lyapunov exponents and inverse participation ratios characterize each trajectory, partition, and vector field. Properties of both vector sets are in quantitative agreement in the long time limit, but finite-time exponent distributions from covariant vectors are narrower than those from Gram-Schmidt vectors, in the range of time scales and total energy examined. Furthermore, the bimodality of the second covariant exponent distributions confirms that ergodicity emerges on different time scales when the trajectory spans different phase space regions. The multimodality of Gram-Schmidt exponent distributions appears to be due, in part, to coordinate dependence. Our results confirm that covariant Lyapunov vectors are time-reversal invariant and show that their finite-time Lyapunov exponent distributions have less dispersion.

PACS numbers: 05.45.Pq, 31.15.xv, 82.20.Wt, 05.45.Jn

## I. INTRODUCTION

Finite-time Lyapunov exponents are statistical observables related to chaos in dynamical systems [1–3]. Exponents estimated from numerical calculations of classical Hamiltonian many-body systems have provided many insights into chaotic dynamics [4, 5]. Lyapunov exponents derive from yet more fundamental objects: tangent bundle vector fields, often called Lyapunov vectors [6, 7]. The nature and utility of various vector fields in numerical calculations has been studied in few degree of freedom systems [8] and spatially extended systems [9–13], such as classical fluids. Relatively little work has focused on the dynamics of finite atomic systems [14], motivating the present study.

The motion of a dynamical system through phase space may be represented numerically by a trajectory composed of discrete points. Initially, nearby trajectories may be locally represented by a tangent vector field composed of a collection of vector sets, each vector set being attached to one point of the reference trajectory [15]. Lyapunov exponents are estimated from the mean rates at which tangent vectors expand or contract over a given time span [16, 17]. The question then, is which vector field one should choose, and how to find it numerically.

Typically, a discretized solution to the linearized equation of motion is used to transport a tangent space vector set at one time to a tangent space at another time [18].

The numerical methodology for finding the vector field then involves transporting and converging an arbitrary set of first variations under the linearized dynamics and perhaps some additional external constraints, such as mutual orthogonality. Quantitative and qualitative properties of Lyapunov exponents and their finite-time distributions depend upon the numerical representation of the vector field, the numerical propagation method, and the dynamical convergence of the propagated vector set.

In this work, we extended a previous analysis [14] of Gram-Schmidt vectors (GSVs) [7, 16, 17] to covariant Lyapunov vectors (CLVs) [8, 9] and their finite-time Lyapunov exponents. For high-dimensional systems, the CLVs are accessible through numerical calculation with either the forward-backward algorithm of Ginelli et al. [9] or the algorithm of Wolfe et al. [8]. In the former method the GS basis is used as a representation of the intrinsic CLV vector set [19, 20]. Given their convergence, CLVs are a coordinate independent basis, time-reversal invariant under the linearized dynamics that coincides with the local stable and unstable manifolds at each point of the trajectory. These characteristics make them important objects for atomic systems, further motivating our work.

Previous studies have examined finite-time exponent distributions for the additional dynamical information contained in their higher moments [21] and their coordinate dependence [22, 23]. It has been shown that these distributions may reflect the emergence of local ergodicity in some systems [24–26]. In the present work we demonstrate that the number of peaks in these distributions may also be affected by the coordinate dependence of the Lyapunov vector set, a phenomenon not found in the distributions of covariant Lyapunov vector expo-

---

\*NSF Postdoctoral Fellow; jg525@cam.ac.uk

†dw34@cam.ac.uk

‡berry@uchicago.edu

nents.

Space-time properties of tangent vector sets are useful in atomic systems for probing the emergence of local ergodicity, as we have previously shown in the Lennard-Jones trimer [24, 26], i.e., three atoms bound by the Lennard-Jones potential. Local ergodicity emerges in the time history of a chaotic trajectory of the trimer when distinct regions of phase space are filled on different time scales [27]. The statistics of tangent vector properties collected in different phase space locales and time spans along a trajectory reflect this phenomenon. The tangent vectors themselves provide additional physical insight into the relevant tangent space directions [14].

In addition to finite-time Lyapunov exponents, another space-time property of Lyapunov vectors is the inverse participation ratio, a localization measure of each Lyapunov vector in the tangent fiber bundle. The ratios give a rough estimate of the inverse number of components contributing to each vector on average, in a given time span. For a range of time scales the ratios provide insight into the space and time localization of tangent vectors, and further aid analysis of the emergence of local ergodicity [14]. Numerically, the tangent space basis vector field quantitatively and qualitatively affects the finite-time Lyapunov exponents and consequently the examination of local ergodicity as it emerges. Here, after describing our computational model and methodology, we reexamine this phenomenon using the stability and localization properties of CLVs.

## II. COMPUTATIONAL MODEL AND METHODOLOGY

Consider a classical mechanical system with a finite number of degrees of freedom,  $s$ . The dynamical state is specified by an  $s$ -tuple  $\mathbf{q} \in M \subseteq \mathbb{R}^s$  of positions in the configuration space  $M$  and an associated  $s$ -tuple of momenta,  $\mathbf{p} \in \mathbb{R}^s$ . Evaluating the Hamiltonian  $H$

$$H(\mathbf{q}, \mathbf{p}) = \frac{1}{2}\mathbf{p}^T \mathbf{Q}^T \mathbf{Q} \mathbf{p} + V(\mathbf{q}) \quad (1)$$

defines a constant energy surface in phase space. The  $s \times s$  matrix  $\mathbf{Q}$  has elements  $Q_{ij} = \delta_{ij}/\sqrt{m_i m_j}$ , where  $m_i$  is the mass of the atom associated with coordinate  $i$ . In the case of a many-body system, such as an atomic cluster, the state may be equivalently specified by the position  $\mathbf{q}_i$  and momenta  $\mathbf{p}_i$ ,  $i = 1, \dots, n$ , which are 3-component vectors for each of the  $n$  atoms. In terms of these 3-component vectors the Lennard-Jones potential function is

$$V(\mathbf{q}) = 4\epsilon \sum_{i < j}^n \left\{ \frac{\sigma^{12}}{|\mathbf{q}_i - \mathbf{q}_j|^{12}} - \frac{\sigma^6}{|\mathbf{q}_i - \mathbf{q}_j|^6} \right\}, \quad (2)$$

where we consider  $n = 3$  atoms, and the center of mass reference frame, Cartesian coordinates, and reduced units were chosen such that  $m_i = 1$ ,  $\sigma = 1$ , and  $\epsilon = 1$ .

Let us denote a phase point as  $\mathbf{x} = (\mathbf{q}, \mathbf{p})^T \in \mathbb{R}^{2s}$ , where  $\mathbf{x}$  is composed of all positions  $\mathbf{q}$  and their linear momenta  $\mathbf{p}$ , and  $s = 3n$  is the number of degrees of freedom. Initially the total energy  $H(\mathbf{q}, \mathbf{p}) = E$  was localized in the symmetric stretch or  $E'$  normal vibrational mode of the global minimum, an equilateral triangular configuration [14]. The normal modes were defined by the eigenvectors of the Hessian (second derivative) matrix. The initial configuration was distorted by displacing the configuration space vector  $\mathbf{q}(t_0)$  of the equilibrium geometry in the Hessian eigenvector direction with the smallest non-zero increase in potential energy. After each configuration space step the potential energy fixed the total energy for the subsequent trajectory.

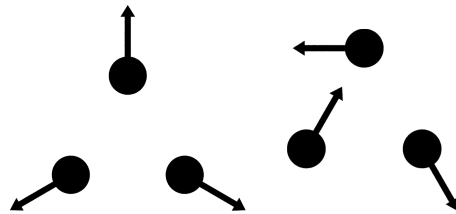


FIG. 1: (Color online) Two normal vibrational modes of the global potential minimum equilateral triangle,  $D_{3h}$ , of the Lennard-Jones trimer. At the potential minimum bond angles are  $60^\circ$  and bond lengths are  $\sqrt[6]{2}\sigma$ . Vectors indicate atomic displacements of (left) the  $A'_1$  symmetric stretch mode and (right) an  $E'$  mode.

Initial excitations and atomic motion were restricted to a two-dimensional plane. The initial conditions  $\mathbf{x}(t_0)$  also fixed the center of mass, linear momentum, and angular momentum at zero, and they remained zero during the simulations. Individual trajectories  $\{\mathbf{x}(t_j) : 0 < j < L\}$  were propagated over  $L$  time steps according to Hamilton's equations using the "velocity Verlet" algorithm [28–30]. The total energy was conserved up to one part in  $10^5$  for millions of time steps. Each time step is  $\tau = t_{j+1} - t_j = 10^{-3}$  in reduced units.

The choice of coordinate system for the configuration space  $M$  endows the tangent space  $T_{\mathbf{x}}M$  at each  $\mathbf{x}$  with a natural coordinate basis  $\{\partial/\partial x^j\}$ ,  $j = 1, \dots, 2s$ . These natural basis vectors are interpreted as local representations of nearby trajectories or perturbations whose time evolution describes the evolution of the orientation of an infinitesimal phase space volume. In numerical calculations these  $2s$  infinitesimal perturbations are instead represented by a new basis set of first variations  $\{\mathbf{g}_i\}$ ,  $i = 1, \dots, 2s$ . Each new basis vector may be expressed in terms of the natural basis set  $\mathbf{g}_i = \sum_j g^{ij} \partial/\partial x^j$  with components  $g^{ij}$ . When propagated and converged under the linearized variational equations with periodic application of the Gram-Schmidt procedure this basis is the Gram-Schmidt (GS) basis. The GS basis is more often written in terms of its components, the natural basis being implied  $\mathbf{g}_i = \{g^{ij}\}$ . We used a linearized form of the

velocity Verlet algorithm for propagation and a method similar to that of Benettin et al. [16, 17] (Appendix A).

The covariant Lyapunov vectors (CLVs)  $\{\mathbf{v}_i\}$  may be expressed in the natural basis as  $\mathbf{v}_i = \sum_j v^{ij} \partial/\partial x^j$  or as  $\{v^{ij}\}$  with the  $j$ th component of the  $i$ th vector being  $v^{ij}$ . They may also be represented in the GS basis  $\mathbf{v}_i = \sum_j c^{ij} \mathbf{g}_j$  with the components  $c^{ij}$ . The latter representation was used by Ginelli [9] to find the CLVs from the GSVs. We followed their method, outlined in Appendix B. Lyapunov exponents were estimated from each set of vectors as described in Appendix C. The  $i$ th GSV and CLV both have the form  $\{\delta q^{ik} \partial/\partial q^k, \delta p^{ik} \partial/\partial p^k\}$ ,  $k = 1, \dots, s$ , where the components of first variations in position and momentum are  $\delta q^{ik}$  and  $\delta p^{ik}$  for the natural basis vectors  $\partial/\partial q^k$  and  $\partial/\partial p^k$ .

Local properties of GSVs and CLVs, such as finite-time Lyapunov exponents, were examined from phase space trajectories partitioned into segments  $\{\mathbf{x}(t_j) : 0 < j < l\}$  of equal length  $l$ . Trajectories with a total length of  $L = 5 \times 10^7$  time steps were divided into  $L/l$  segments. Spectra of finite-time Lyapunov exponents and inverse participation ratios were calculated from vector sets propagated over each time segment. Finite-time Lyapunov exponents are denoted  $\{\lambda_i(\mathbf{x}_0, l)\}$  and inverse participation ratios are denoted  $\{Y_i(\mathbf{x}_0, l)\}$  to indicate their dependence on  $\mathbf{x}_0 \equiv \mathbf{x}(t_0)$ , the initial phase point of the time segment, and  $l$ , the length of the time segment. Below,  $\lambda_i$  and  $Y_i$  refer to finite-time quantities. Distributions  $\{f(\lambda_i, l)\}$  and  $\{f(Y_i, l)\}$ ,  $i = 1, \dots, 2s$  were generated for each partition of trajectories at each total energy.

The structure of GSVs and CLVs was also probed with a modified mean inverse participation ratio  $Y$ . Over a trajectory segment of length  $l$  this ratio measures localization of the GSVs [19, 20] in the tangent bundle. For the  $i$ th vector  $\mathbf{z}_i$  (GSV or CLV) we take the mean inverse participation ratio to be

$$Y_i = \left\langle N^2 \sum_{k=1}^s (z^{ki}(t_j))^4 \right\rangle \quad (3)$$

where  $z^{ki}$  is the  $k$ th component of the  $i$ th vector,  $(z^{ki})^2 \equiv (\delta q^{ki})^2 + (\delta p^{ki})^2$ , the brackets indicate an average over the number of time steps in the trajectory (or trajectory segment), and the normalization factor  $N$  is  $1/\sum_{k=1}^s (z^{ki}(t_j))^2 = 1$ . Evaluating  $\{Y_i\}$  gives a rough estimate of the average inverse number of degrees of freedom contributing to each vector over a time span. On average, a normalized, purely delocalized vector would have all components equal to  $1/\sqrt{2s}$ , while a normalized, purely localized vector would have one nonzero component equal to unity. Hence, a localized vector has a  $Y$  around unity, while a delocalized vector has  $Y$  closer to  $1/s$ . The indices correspond to the associated Lyapunov vector and Lyapunov exponent.

### III. NUMERICAL RESULTS AND ANALYSIS

Figure 2 shows  $f(\lambda_1, l)$  distributions for GSVs and CLVs over a range of time segment lengths. These results are for a trajectory in which the symmetric stretch was initially excited to a total energy of  $E = -1.673 \epsilon$ . The areas under these distributions are normalized to unity. For reference, the global minimum equilateral triangle configuration has a potential energy of  $-3.000 \epsilon$  and the linear stationary point has an energy of  $-2.031 \epsilon$ . Most striking in Figure 2 are the CLV exponent distributions in panel (b), which are essentially identical over the range of time scales examined. Though they are not shown, similar results were obtained for  $f(\lambda_2, l)$  and distributions for initial excitations of an  $E'$  vibrational mode.

Each peak in Figure 2 (b) is also significantly narrower than any GS distribution. Previous work has shown that as the length  $l$  of the trajectory segments is increased, the distribution of finite-time GS exponents narrows, eventually converging to the asymptotic value [14, 31]. For GSVs, all total energies, segment lengths, and initially excited modes,  $f(\lambda_1, l)$  and  $f(\lambda_{18}, l)$  are symmetric about the  $\lambda = 0$  axis, as are  $f(\lambda_2, l)$  and  $f(\lambda_{17}, l)$ .

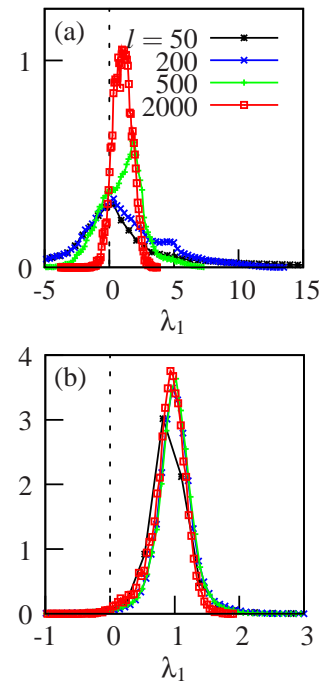


FIG. 2: (Color online) The  $\lambda_1$  distribution  $f(\lambda_1, l)$  for (a)  $\mathbf{g}_1$  and (b)  $\mathbf{v}_1$  over a range of time segment lengths  $l = 50$  (\*), 200 (x), 500 (+), 2000 (□) along the same trajectory. The total energy  $E = -1.673 \epsilon$  was initially deposited in the symmetric stretch of the global minimum equilateral triangle.

Finite-time Lyapunov exponents quantify the average rates of expansion and contraction in the directions of the

chosen vector set in each time segment. Expanding vectors pointing in diverging directions have positive finite-time Lyapunov exponents ( $\lambda_1$  and  $\lambda_2$ ) and contracting or converging directions have negative finite-time Lyapunov exponents ( $\lambda_{17}$  and  $\lambda_{18}$ ). Thus, at least in part, the multimodality of GSV distributions may be caused by coordinate dependent expansions and contractions canceling when they occur on time scales shorter than that of the time segment [32]. The covariant result then suggests that CLV exponents properly capture the local stretching (contracting) rates along the unstable (stable) manifolds in phase space.

The mean inverse participation ratio distributions,  $f(Y_i, l)$ , were also calculated for each trajectory. For both vector sets, at all total energies and time segment lengths,  $f(Y_1, l)$  and  $f(Y_{18}, l)$  are identical, as are  $f(Y_2, l)$  and  $f(Y_{17}, l)$ . Only results for  $Y_1$  are shown in Figure 3, at  $E = -1.673\epsilon$  and several time segment lengths, to demonstrate that the distributions for corresponding GSVs and CLVs are also identical.

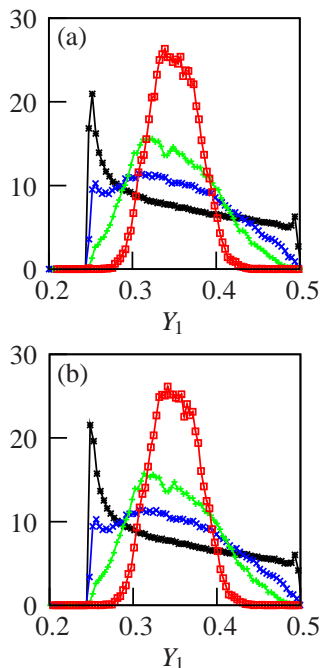


FIG. 3: (Color online) The  $Y_1$  distribution  $f(Y_1, l)$  for (a)  $\mathbf{g}_1$  and (b)  $\mathbf{v}_1$  over a range of time segment lengths  $l = 50$  (\*), 200 ( $\times$ ), 500 (+), 2000 ( $\square$ ) along the same trajectory. The total energy  $E = -1.673\epsilon$  was initially deposited in the symmetric stretch of the global minimum equilateral triangle.

Distributions for both vector sets undergo qualitative changes over the range of time scales examined. In particular, these distributions are narrow for longer time segments, suggesting that  $\mathbf{g}_1$  and  $\mathbf{v}_1$  are more localized over longer time spans. In finite time segments the value of

each inverse participation ratio realization measures the degree of localization. With Figure 2 these results suggest that the inverse participation ratio and Lyapunov exponent distributions, component localization and stability, need not be correlated.

Given a partitioned trajectory, GSVs and CLVs may be more localized (larger inverse participation ratio) in some time segments and more delocalized (smaller inverse participation ratio) in others. Fluctuations in the degree of localization, in terms of components, are reflected in the distributions  $f(Y_i, l)$ . From the identical GSV and CLV inverse participation ratio distributions we conclude that their components are similarly localized in trajectory tangent fiber bundles. Figure 2 shows that while they are similarly localized their associated finite-time exponents are quite different.

Qualitatively, in the range of timescales and total energy examined, exponent distributions from CLVs are narrower than those from GSVs. That the CLV exponent distributions have less dispersion was apparent at all total energies examined. Figures 4 and 5 show CLV  $\lambda$  distributions  $f(\lambda, 200)$  at several total energies for initial symmetric stretch and  $E'$  mode excitations. In both  $\lambda_1$  and  $\lambda_2$  GSV exponent distributions, multimodality was present at total energies above the potential energy of the linear saddle [14]; this result suggests that local ergodicity emerges on different time scales for these trajectories [14]. The bimodality of the CLV exponent distributions  $f(\lambda_2, 200)$  when the trajectory spans different phase space regions confirms this hypothesis and suggests that the multimodality of GSV exponent distributions is partly due to the coordinate dependence of GSVs.

Peaks in  $f(\lambda_2, 200)$  reflect the separation of motion into a region of highly chaotic behavior, characterizing motion in the potential well, and a region with much more regular dynamics, characterized by a longer time scale, corresponding to motion across the saddles [33]. The CLV exponent distribution  $f(\lambda_1, 200)$  is only bimodal at the highest total energy, reflecting bound motion and motion near the dissociation threshold. The remaining peaks in the GS exponent distributions observed over a wide energy range and time segment length, are thus, in part, due to the coordinate dependence of GSVs reflecting characteristics of directions associated with both the local stable and unstable manifolds.

At all total energies in the long time limit, Lyapunov exponents and inverse participation ratios of both vector basis sets are generally in quantitative agreement. By iterating over trajectory segments that are mechanically reversible (shorter than  $10^5$  steps), we confirmed that CLVs are time-reversal invariant. For initial excitations of the symmetric stretch and  $E'$  modes, the mean of the  $f(\lambda, 200)$  distributions decreases at total energies just above the potential energy of the linear saddle. This finding is in agreement with long time results found previously [14] and confirmed here.

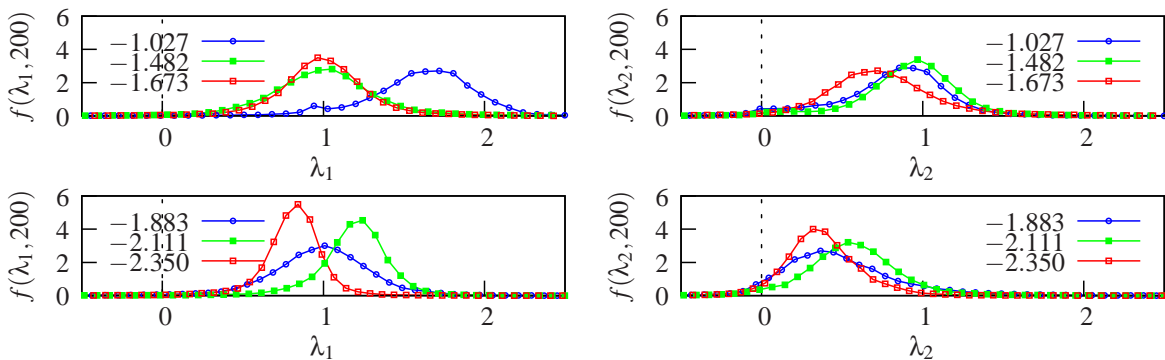


FIG. 4: (Color online) Covariant Lyapunov exponent  $\lambda_1$  and  $\lambda_2$  distributions  $f(\lambda_1, 200)$  and  $f(\lambda_2, 200)$  from trajectories at different total energies.  $\lambda_1$  and  $\lambda_2$  were collected from 200 time step segments. The total energy of each trajectory was initially deposited in the symmetric stretch of the equilateral triangle configuration.

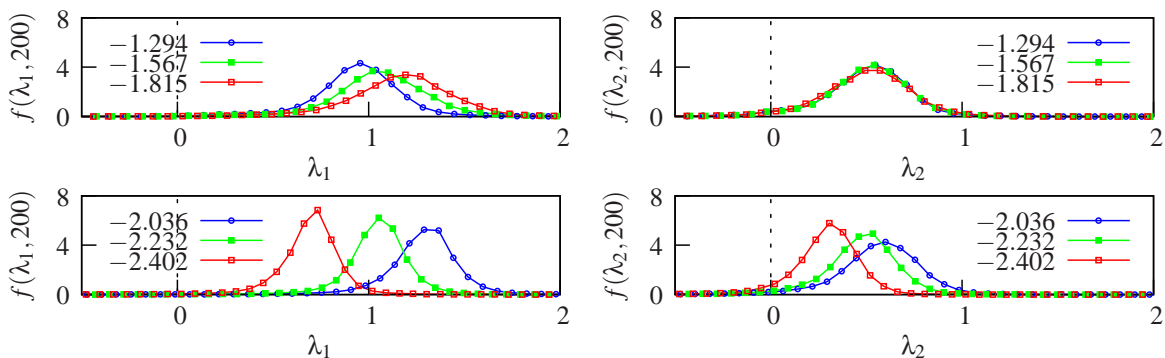


FIG. 5: (Color online) Covariant Lyapunov exponent  $\lambda_1$  and  $\lambda_2$  distributions  $f(\lambda_1, 200)$  and  $f(\lambda_2, 200)$  from trajectories at different total energies.  $\lambda_1$  and  $\lambda_2$  were collected from 200 time step segments. The total energy of each trajectory was initially deposited in the  $E'$  mode of the equilateral triangle configuration.

#### IV. CONCLUSIONS

Space-time properties measuring stability and localization characterizing Gram-Schmidt and covariant Lyapunov sets were used to probe the tangent space directions that determine the time evolution of the Lennard-Jones trimer. Our results demonstrate that CLVs are more appropriate than GSVs for estimation of finite-time Lyapunov exponents. The coordinate independence of the CLVs produces associated finite-time exponent distributions with means and moments that depend only upon the initial conditions. These distributions clearly reveal the emergence of local ergodicity in phase space and permit a more accurate estimate of the separate time scales involved in this phenomenon.

#### V. ACKNOWLEDGEMENTS

J.R.G. acknowledges support from the National Science Foundation (OISE-0700911).

#### Appendix A: Gram-Schmidt vectors

At the initial phase point  $\mathbf{x}(t_0)$  of a trajectory, a set of first variations are defined as orthonormal, column vectors,  $\{\mathbf{u}_i(t_0)\}$ ,  $i = 1, \dots, 2s$ . Propagated in time, and periodically orthogonalized, this vector set becomes  $\mathbf{G}(t) = \{\mathbf{g}_i(t)\}$ , the Gram-Schmidt (GS) basis at time  $\mathbf{x}(t)$ . Members of the basis are Gram-Schmidt vectors (GSVs). Each member has the form  $\mathbf{g}_i = (\delta\mathbf{q}, \delta\mathbf{p})^T \in T_{\mathbf{x}}M^{2s} \subset T_{\mathbf{x}}\mathbb{R}^{2s}$ . For sufficiently large  $t_m$ , where  $t_0 \ll t_m < t_L$ , the GS basis  $\{\mathbf{g}_i(t_m)\}$  depends only on the phase point  $\mathbf{x}(t_m)$ . The GSVs lie in the tangent space  $T_{\mathbf{x}}M^{2s}$  attached to each phase point  $\mathbf{x}$ .

The GS basis is propagated forward in time, concurrently with the phase point, using the discretized form of the integrated, linearized equation of motion

$$\bar{\mathbf{g}}_i(t_j) = \mathbf{M}(t_j, t_{j-1}) \mathbf{g}_i(t_{j-1}). \quad (\text{A1})$$

The propagator  $\mathbf{M}(t_j, t_{j-1})$ , in the linearized form of the

velocity Verlet algorithm, is the matrix product

$$\begin{pmatrix} \mathbf{I} & \mathbf{0} \\ -\frac{\tau}{2}\mathbf{H}(t) & \mathbf{I} \end{pmatrix} \begin{pmatrix} \mathbf{I} & \mathbf{T} \\ \mathbf{0} & \mathbf{I} \end{pmatrix} \begin{pmatrix} \mathbf{I} & \mathbf{0} \\ -\frac{\tau}{2}\mathbf{H}(t_{j-1}) & \mathbf{I} \end{pmatrix}, \quad (\text{A2})$$

where  $[\mathbf{T}]_{kl} = \tau \delta_{kl}/m_k$ ,  $\delta_{kl}$  is the Kronecker delta,  $\mathbf{I}$  is the identity matrix, and  $\mathbf{H}$  is the mass-weighted Hessian matrix

Gram-Schmidt orthogonalization is actually a method of implementing a QR decomposition [2]. Any matrix  $\mathbf{A}$  may be decomposed into an orthogonal matrix  $\mathbf{Q}$  and an upper triangular matrix  $\mathbf{R}$

$$\mathbf{A} = \mathbf{Q}\mathbf{R}. \quad (\text{A3})$$

Applying this decomposition to the propagated GS basis, after a single time step the propagated basis is

$$\overline{\mathbf{G}}(t_j) = \mathbf{Q}(t_j)\mathbf{R}(t_j) \quad 1 \leq j \leq L \quad (\text{A4})$$

$$= \mathbf{M}(t_j, t_{j-1})\mathbf{G}(t_{j-1}) \quad (\text{A5})$$

$$= \mathbf{M}(t_j, t_{j-1})\mathbf{Q}(t_{j-1}) \quad (\text{A6})$$

where the first equality is the QR decomposition and the last equality follows because the  $j$ th GS basis is taken to be the columns of  $\mathbf{Q}(t_j)$  (i.e.,  $\mathbf{G}(t_j) = \mathbf{Q}(t_j)$ ).

For  $L$  successive time steps, the tangent space propagator  $\mathbf{M}(t_L, t_0)$  is a matrix product of single time step propagators

$$\mathbf{M}(t_L, t_0) = \prod_{j=1}^L \mathbf{M}(t_j, t_{j-1}). \quad (\text{A7})$$

After  $L$  steps the propagated basis is then

$$\overline{\mathbf{G}}(t_L) = \mathbf{M}(t_L, t_0)\mathbf{Q}(t_0) = \mathbf{Q}(t_L)\mathbf{R}(t_L) \quad (\text{A8})$$

where  $\mathbf{R}(t_L) = \mathbf{R}(t_{L-1})\dots\mathbf{R}(t_0)$ ; the product of any number of upper triangular matrices is upper triangular. Diagonal elements  $[\mathbf{R}]_{ii}$  are equivalent to  $\|\mathbf{g}_i\|$ . Off-diagonal, non-zero elements of  $\mathbf{R}(t_j)$  are obtained by projecting each vector  $\overline{\mathbf{g}}_i(t_j)$  onto the subspace spanned by  $\{\overline{\mathbf{g}}_k(t_j)\}$  with  $k < i$ . These elements are typically discarded, but in the present work are used in the calculation of covariant Lyapunov vectors.

### Appendix B: covariant Lyapunov vectors

Here we outline the algorithm of Ginelli et al. [9]. Assume a GS basis has been generated at  $t_m$ . As the GS basis is propagated forward from  $t_m$  to  $t_L$ , the matrices  $\mathbf{R}^{-1}$  and  $\mathbf{Q}$  are stored at each time step. These matrices are used in backward iterations from  $t_L \rightarrow t_m$  to extract the covariant Lyapunov vectors (CLVs). At  $t_L$ , we take a similar approach to that used to find the GS basis and also define an arbitrary vector set  $\mathbf{W}(t_L) = \{\mathbf{w}_i(t_L)\}$ . Each vector  $\mathbf{w}_i(t_L)$  is a generic linear combination of  $\{\mathbf{g}_j(t_L)\}$ ,  $j = 1, \dots, i$  (i.e., the first  $i$  GSV at time  $t_L$ ). In practice it is more convenient to define and work with the components  $c_{ij}(t_L)$  of  $\mathbf{w}_i(t_L)$  in the GS basis, namely  $\mathbf{g}_j(t_L)^T \mathbf{w}_i(t_L)$ . The vector set  $\mathbf{W}(t_L)$  in the GS basis has components  $\mathbf{C}(t_L) = \mathbf{G}^T(t_L)\mathbf{W}(t_L)$ . The matrix  $\mathbf{C}(t_L)$

is set to the  $2s \times 2s$  identity matrix but may be any arbitrary upper triangular matrix.

The matrix  $\mathbf{C}(t_L)$  is propagated backward in time from  $t_L$  to  $t_m$  as

$$\mathbf{C}(t_{k-1}) = \mathbf{R}(t_{k-1})^{-1}\mathbf{C}(t_k), \quad (\text{B1})$$

which is tantamount to propagating  $\mathbf{W}$  in the GS basis. Performing this propagation sufficiently far backward in time,  $t_m \leftarrow t_L$ ,  $t_m \ll t_L$ , each  $\mathbf{w}_i(t_L)$  aligns with the most (backward) expanding direction within the appropriate covariant subspace. If  $t_L - t_m$  is sufficiently large, the covariant vector set  $\mathbf{V}(t_m)$  is

$$\mathbf{V}(t_m) = \mathbf{G}(t_m)\mathbf{C}(t_m). \quad (\text{B2})$$

The covariant Lyapunov vectors  $\mathbf{V}$  thus depend on the convergence of  $\mathbf{U} \rightarrow \mathbf{G}$  and  $\mathbf{W} \rightarrow \mathbf{V}$ .

Since  $\mathbf{R}\mathbf{R}^{-1} = \mathbf{R}^{-1}\mathbf{R} = \mathbf{I}$  we also have  $\mathbf{C}(t_m) = \mathbf{R}(t_{m-1})\mathbf{C}(t_{m-1})$ . Multiplying both sides by  $\mathbf{Q}(t_m)$  and substituting  $\overline{\mathbf{G}}(t_m) = \mathbf{Q}(t_m)\mathbf{R}(t_m)$ ,

$$\mathbf{V}(t_m) = \mathbf{M}(t_m, t_{m-1})\mathbf{V}(t_{m-1}). \quad (\text{B3})$$

This is the equation of motion for the CLVs.

### Appendix C: Lyapunov exponents

The spectrum of Lyapunov exponents is estimated from the GS basis using the Euclidean norms  $\{\|\mathbf{g}_i\|\}$  stored after GS orthogonalization of the GS basis with respect to  $\|\mathbf{g}_1\|$ . Exponents depend on the norm used [34]. The  $i$ th exponent over a finite time  $t_L - t_0$  is

$$\begin{aligned} \lambda_i(t_L, t_0) &= \langle \ln \|\mathbf{g}_i(t)\| \rangle_t \\ &= \frac{1}{t_L - t_0} \sum_{j=1}^L \ln \|\mathbf{g}_i(t_j)\|, \end{aligned} \quad (\text{C1})$$

in natural units per reduced time for the  $i$ th GSV. The difference  $t_L - t_0 = L\tau$ . The covariant Lyapunov exponents are calculated from the backward iteration using the cumulative average

$$\begin{aligned} \lambda_i(t_0, t_L) &= \langle \ln \|\mathbf{v}_i(t)\| \rangle_t \\ &= \frac{1}{t_0 - t_L} \sum_{j=0}^L \ln \|\mathbf{v}_i(t_j)\|, \end{aligned} \quad (\text{C2})$$

where the average is over accumulated time. This time average is different from that used for Lyapunov exponents estimated from GSVs. The  $\mathbf{R}$  matrix at time  $t_k$  is  $\mathbf{R}(t_k) = \mathbf{R}(t_{k-1})\dots\mathbf{R}(t_0)$ , implicitly carrying the  $\mathbf{R}$  matrices at each step along the forward iteration. Using these matrices in the backward iteration to extract  $\mathbf{V}$  then requires each  $t_l$  to be

$$t_l = \tau \sum_{i=1}^l i = \frac{\tau}{2} l(l+1).$$

- 
- [1] H. Fujisaka, Prog. Theor. Phys. **70**, 1264 (1983).
- [2] J.-P. Eckmann and D. Ruelle, Rev. Mod. Phys. **58**, 617 (1985).
- [3] B. Eckhardt and D. Yao, Physica D **65**, 100 (1993).
- [4] H. Posch and W. Hoover, J. Phys.: Conf. Ser. **31**, 9 (2006).
- [5] R. S. Berry, Adv. Chem. Phys. **130**, 3 (2005).
- [6] B. Legras and R. Vautard, in *1995 ECMWF Seminar on Predictability*, edited by T. Palmer (143-156, Reading, UK, 1996).
- [7] A. Trevisan and F. Pancotti, J. Atmos. Sci. **55**, 390 (1998).
- [8] C. L. Wolfe and R. M. Samelson, Tellus **59A**, 355 (2007).
- [9] F. Ginelli, P. Poggi, A. Turchi, H. Chaté, R. Livi, and A. Politi, Phys. Rev. Lett. **99**, 130601 (2007).
- [10] H. Yang, K. A. Takeuchi, F. Ginelli, and H. C. and Günter Radons, Phys. Rev. Lett. **102**, 074102 (2009).
- [11] D. Pazó, I. G. Szendro, J. M. López, and M. A. Rodríguez, Phys. Rev. E **78**, 016209 (2008).
- [12] I. G. Szendro, D. Pazó, M. A. Rodríguez, and J. M. López, Phys. Rev. E **76**, 025202 (2007).
- [13] C. L. Wolfe and R. M. Samelson, J. Atmos. Sci. **65**, 875 (2008).
- [14] J. R. Green, J. Jellinek, and R. S. Berry, Phys. Rev. E **80**, 066205 (2009).
- [15] B. Leimkuhler and S. Reich, *Simulating Hamiltonian Dynamics*, Cambridge Monographs on Applied and Computational Mathematics (Cambridge University Press, 2004).
- [16] G. Benettin, L. Galgani, A. Giorgilli, and J.-M. Strelcyn, Meccanica **15**, 9 (1980).
- [17] G. Benettin, L. Galgani, A. Giorgilli, and J.-M. Strelcyn, Meccanica **15**, 21 (1980).
- [18] G. Casati, B. V. Chirikov, and J. Ford, Phys. Lett. **77A**, 91 (1980).
- [19] H. Yang and G. Radons, Phys. Rev. E **71**, 036211 (2005).
- [20] G. Radons and H. Yang, *Static and dynamic correlations in many-particle Lyapunov vectors* (2004), URL <http://arxiv.org/abs/nlin/0404028>.
- [21] C. Froeschlé, C. Froeschlé, and E. Lohinger, Celest. Mech. Dyn. Astron. **56**, 307 (1993).
- [22] Y. Elskens, Physica D **100**, 142 (1997).
- [23] A. Prasad and R. Ramaswamy, Phys. Rev. E **60**, 2761 (1999).
- [24] T. L. Beck, D. M. Leitner, and R. S. Berry, J. Chem. Phys. **89**, 1681 (1988).
- [25] C. Amitrano and R. S. Berry, Z. Phys. D **26**, 388 (1993).
- [26] C. Amitrano and R. S. Berry, Phys. Rev. E **47**, 3158 (1993).
- [27] C. Amitrano and R. S. Berry, Phys. Rev. Lett. **68**, 729 (1992).
- [28] W. C. Swope, H. C. Andersen, P. H. Berens, and K. R. Wilson, J. Chem. Phys. **76**, 637 (1982).
- [29] L. Verlet, Phys. Rev. **159**, 98 (1967).
- [30] A. Iserles, *A First Course in the Numerical Analysis of Differential Equations*, Cambridge Texts in Applied Mathematics (Cambridge University Press, 2008), 2nd ed.
- [31] H. Abarbanel, R. Brown, and M. Kennel, J. Nonlinear Sci. **1**, 175 (1991).
- [32] D. J. Wales and R. S. Berry, J. Phys. B: At. Mol. Opt. Phys. **24**, L351 (1991).
- [33] R. J. Hinde, D. J. Wales, and R. S. Berry, J. Chem. Phys. **96**, 1376 (1992).
- [34] A. Pikovsky and A. Politi, Nonlinearity **11**, 1049 (1998).